Modelling and experimental verification of tip-induced polarization in Kelvin probe force microscopy measurements on dielectric surfaces

Nielsen, Dennis Achton; Popok, Vladimir; Pedersen, Kjeld

Published in:
Journal of Applied Physics

DOI (link to publication from Publisher):
10.1063/1.4935811

Publication date:
2015

Document Version
Publisher's PDF, also known as Version of record

Modelling and experimental verification of tip-induced polarization in Kelvin probe force microscopy measurements on dielectric surfaces

Dennis A. Nielsen, Vladimir N. Popok, and Kjeld Pedersen

Citation: Journal of Applied Physics **118**, 195301 (2015); doi: 10.1063/1.4935811
View online: http://dx.doi.org/10.1063/1.4935811
View Table of Contents: http://scitation.aip.org/content/aip/journal/jap/118/19?ver=pdfcov
Published by the AIP Publishing

Modelling and experimental verification of tip-induced polarization in Kelvin probe force microscopy measurements on dielectric surfaces

Dennis A. Nielsen,[a] Vladimir N. Popok, and Kjeld Pedersen
Department of Physics and Nanotechnology, Aalborg University, 9220 Aalborg East, Denmark

(Received 9 September 2015; accepted 2 November 2015; published online 16 November 2015)

Kelvin probe force microscopy is a widely used technique for measuring surface potential distributions on the micro- and nanometer scale. The data are, however, often analyzed qualitatively, especially for dielectrics. In many cases, the phenomenon of polarization and its influence on the measured signals is disregarded leading to misinterpretation of the results. In this work, we present a model that allows prediction of the surface potential on a metal/polymer heterostructure as measured by Kelvin probe force microscopy by including the tip-induced polarization of the dielectric that arises during measurement. The model is successfully verified using test samples. © *2015 AIP Publishing LLC*. [http://dx.doi.org/10.1063/1.4935811]

I. INTRODUCTION

In recent years, the fields of application of scanning probe microscopy (SPM) significantly expanded in terms of capabilities to measure a broad spectrum of parameters of surfaces and nanostructures.[1–4] In the family of SPM, Kelvin Probe Force Microscopy (KPFM) provides the possibility to find local distributions of surface electric potentials.[5–7] This technique is widely used on conducting and semiconducting surfaces, where it is well supported theoretically and can therefore give quantitative data regarding electronic structure of the surface, for instance, the local work function difference in metals, local dopant concentration or electronic band bending in semiconductors.[8–10]

KPFM also attracted a lot of attention in studies of thin dielectric films, multi-layered systems, heterointerfaces as well as biological objects, showing spatial resolution down to the nanoscale.[11–15] In this case, the obtained KPFM images are often interpreted in terms of the work function difference between the tip and conducting back-plate supporting the insulator, assuming that the presence of the dielectric medium modifies the KPFM signal.[16] However, these changes in the measured potential are typically treated qualitatively, for example, through variations in charge density. Moreover, the surface potential maps experimentally obtained on heterostructures such as organic field-effect transitors, capacitors, and solar cells are often interpreted as actual ones[13,17,18] disregarding additional electric fields introduced by the tip affecting the measured signal. This influence of the tip has two main impacts. One of them is polarization of the dielectric or formation of dipoles. These phenomena have started to be recognized in some recent studies, see, for example, Ref. 19. However, the other impact factor—which is the tip position, defining the value of the electric field—is still not taken into account in KPFM studies.

We expect that the presence of the tip not only changes the value of the measured potential but also causes change in the potential gradients at interfaces of a dielectric with metal (conductive) contacts, which has been treated as contact resistance and the presence of Schottky barriers.[13,17] In some KPFM measurements, it has previously been practiced to get the actual surface potential distribution by subtracting the surface potential measured on the grounded sample from that measured on the biased one.[17] Despite this procedure seems like an intuitive approximation, it may cause incorrect interpretation of the results. The weak point lies in the fact that the surface potential distribution is affected by the tip position, which changes the gradients as will be shown below.

To our best knowledge, polarization of the dielectrics and change in the electric field distribution due to the potential applied to the tip have never been treated quantitatively for KPFM measurements and an appropriate theory is missing. In this paper, we show how to include electrostatic forces due to the tip-induced polarization into the solution of the equations for the capacitive forces between the tip and dielectric surface, thus taking into account corresponding changes of the surface potential. The developed approach is used for prediction of the surface potential distribution measured by KPFM on a metal/dielectric heterostructure, and it is experimentally verified on test samples.

II. EXPERIMENTAL METHOD

A. Test sample fabrication

The test samples are designed to consist of two grids of interleaving aluminum stripes (see Fig. 1) produced on a glass substrate. The thickness of the stripes is 100 nm, the width is 7 μm, and the periodicity is 20 μm. The entire structure is covered by approximately 200 nm thick film of poly(methyl methacrylate) (PMMA). The mask for the grid is produced by a standard lithography procedure and the aluminum is deposited by sputter coating. The PMMA film is formed by spin-coating. Finally, wires are connected to both grids by soldering to provide electrical connections.

[a]Electronic mail: dan@nano.aau.dk

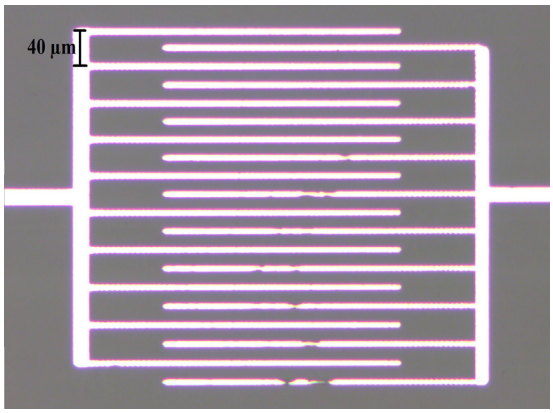

FIG. 1. Top-view optical microscopy image of the aluminum grid geometry.

B. KPFM measurements

The samples are investigated by atomic force microscopy (AFM) in tapping mode and KPFM using an NTEGRA Aura nanolaboratory from NT-MDT. Standard NSG01/Pt type PtIr coated cantilevers with tip curvature radius around 35 nm are used for both topography and surface potential measurements. A two-pass scan mode is applied, where the topography is measured during the first pass and the surface potential during the second one. The topography measured in the first pass is used to keep a constant tip-to-sample distance of 10 nm during the second pass. In the KPFM pass an AC voltage of frequency ω is applied between the tip and sample. Additionally, a varying DC voltage is also applied. The resulting force on the tip at frequency ω is given by[8]

$$F_\omega = -\frac{\partial C}{\partial z}[\Delta\phi - V_{DC}] \cdot V_{AC}\sin(\omega t), \tag{1}$$

where C is the tip/sample capacitance, z is the tip-to-sample distance, and $\Delta\phi$ is the potential difference between the tip and the sample at the scan point. F_ω is nullified by adjusting V_{DC} so that it matches $\Delta\phi$ in each scan point. V_{DC} is then recorded for each scan point and used to generate the surface potential distribution. The measured surface potentials should be interpreted according to the type of material under investigation. On conducting surfaces, $\Delta\phi$ corresponds to the difference in work functions, also known as the contact potential difference (CPD), between the tip metal coating and the sample. When applying KPFM to semiconducting or insulating materials, the measurements can be affected by band bending, formation of surface dipoles, or the presence of local charges. An important factor to consider is the local polarization field introduced by the tip as already mentioned in the Introduction and stressed in Ref. 19.

III. MODELLING

In order to explain the surface potential distributions measured by KPFM on the test samples, a three-dimensional finite element model of the tip/sample system is constructed. The model enables simulation of the electric potential distribution at the sample surface as measured by the tip, as well as the potential distribution at the same applied voltage, but without the presence of the tip. Hence, the main purpose of the model is to verify the assumption that the measured surface potential distribution is heavily affected by the tip-induced polarization of the dielectric film.

A. Method

The simulations are carried out using COMSOL Multiphysics version 4.3. The sample in the model has the same geometry as the test sample (see details below). The model geometry, shown in Fig. 2, is divided into a tetrahedral mesh. The mesh around the tip apex is refined with a maximum mesh size of 50 nm in order to improve the resolution of the surface potential in the area around the tip. In practice, it is done by placing a 1 μm $\times$ 1 μm $\times$ 0.5 μm box around the tip and refining the mesh only within that box (referred to as "tip box" in Table I) in order to reduce the total number of elements. The total mesh is constructed using the parameters listed in Table I.

The model utilizes a stationary electrostatic simulation that solves the Poisson equation

$$\varepsilon_r(x,y,z)\varepsilon_0\nabla^2\phi(x,y,z) = -\rho(x,y,z), \tag{2}$$

where ε_r is the dielectric constant, ε_0 is the vacuum permittivity, ϕ is the electrostatic potential, and ρ is the charge density. Eq. (2) is solved using a set of boundary conditions as a starting point in order to obtain the spatial potential distribution $\phi(x,y,z)$. It is assumed that the system does not contain free charges, and therefore, the charge density ρ is set to zero in the model equation.

The polarization field can be determined from the electric potential distribution by

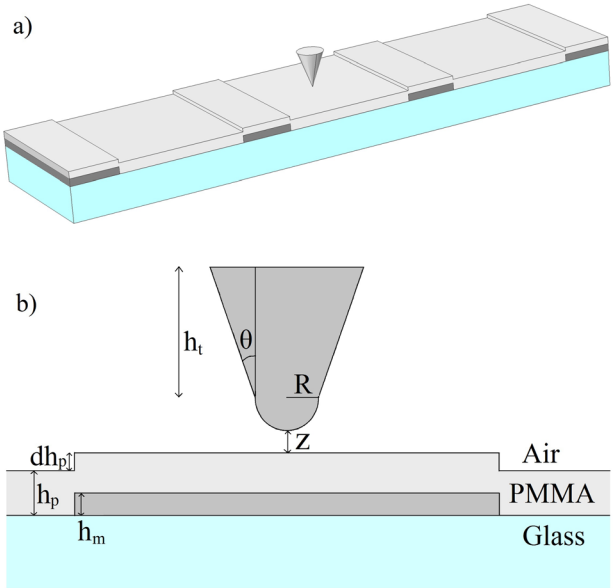

FIG. 2. (a) 3D overview image of the model geometry and (b) 2D inset of the geometry, where z is the tip-sample distance, R is the tip curvature radius, θ is the half-aperture angle, h_t is the height of the tip, h_m is the aluminum film thickness, h_p is the thickness of the PMMA film, and dh_p is the height difference between the areas with and without metal stripes, respectively.

TABLE I. Mesh details of the tip/sample geometry. The number of elements may vary slightly depending of the tip position.

Area	Mesh type	Min. size (nm)	Max. size (nm)	No. elements
Tip apex	Triangular	2	5	778
Tip side	Triangular	2	60	31×10^3
Tip box	Tetrahedral	2	50	77×10^3
PMMA film	Tetrahedral	2	500	82×10^3
Glass/air	Tetrahedral	2	2000	414×10^3
		Total number of elements		610×10^3

$$\bar{P}(x,y,z) = (1-\varepsilon_r)\varepsilon_0 \bar{\nabla}\phi(x,y,z). \quad (3)$$

This polarization field will cause high potential gradients at the edges of metal stripes during KPFM measurements, because its strength decreases with distance squared. The divergence of the polarization field corresponds to the polarization charge density, which according to Ref. 19 has an impact on the measured surface potential.

The tip domain and metal stripe domains are excluded from the modelling domains, because it is assumed that the electric potential is constant within these domains. Hence, only their surfaces are meshed, and the potential at the boundaries of these domains is set correspondingly to the potential applied during the experiment.

Two simulation sets are carried out representing the KPFM measurements on the grounded and biased sample, respectively. In the first set, the potential at the tip boundary is 2.05 V, as measured during experiments (see Section IV), and all the metal boundaries are at 0 V representing electrical ground. In the second set, the potential at the boundaries of every second metal stripe domain is changed to 3 V, while the rest of the boundary conditions from the first set is kept.

In both simulation sets, the three-dimensional electric potential distributions are calculated for 41 tip positions placed equidistantly on a line between the centres of two neighboring metal stripes. At every position, the tip-to-sample distance is kept at $z = 10$ nm. The generated surface potential profile along the scan line is recorded for every tip position, and, along with a point spread function (PSF), the simulated/predicted surface potential is generated for every scan point. There is no fitting involved in the simulation procedure. Finally, a single simulation is performed without the presence of the tip in order to emphasize the effect of the tip on the measured surface potential during KPFM.

B. Model geometry

The model geometry includes the cantilever tip, PMMA film, aluminum stripes in the same configuration as in the test samples, and the glass substrate. An overview of the geometry is shown in Fig. 2. In the model, a box is added around the entire structure in order to determine a model domain. The values of the geometric and material parameters are listed in Table II.

The parameters w_m, w_p, h_m, and dh_p are measured by AFM. The thickness of the PMMA layer h_p is found on an area without aluminum. The tip apex radius of 35 nm is acquired from the manufacturer data sheet. The tip height is, according to the manufacturer, 14–16 μm. The reason for only including the bottom 5 μm of the tip in the model is that the electric field at the apex affects the most the surface potential distribution. According to the work by Elias *et al.*,[20] the upper part of the cantilever tip contributes very little to the KPFM measurement. However, the cantilever beam, according to their work, may have an effect on the measured absolute value of CPD, because the cantilever beam can be affected by the electric potential applied to the sample and thus introduce changes in CPD. However, the beam is not expected to have any significant impact on how the dielectric is polarized by the tip at and around the scan point, which serves as a justification for the exclusion of the cantilever beam from this model.

TABLE II. Geometric and material parameters of the model. The values are chosen in order to mimic the tip-sample system of the KPFM measurements on the test samples.

Parameter	Value	Description
w_m	7 μm	Width of metal stripes
w_p	13 μm	Distance between metal stripes
h_m	100 nm	Aluminum film thickness
h_p	200 nm	PMMA film thickness
dh_p	90 nm	PMMA film height difference
ε_P	2.6	Dielectric constant of PMMA
ε_G	5	Dielectric constant of glass
z	10 nm	Tip-to-sample distance
R	35 nm	Tip apex radius
h_t	5 μm	Tip height
Θ	15 deg	Tip half-aperture angle
CPD	2.05 V	Contact potential difference

C. Point spread function

The surface potential measured at a given point during KPFM is not the exact surface potential at that point, but rather a weighted sum of the potential at and surrounding the scan points. The weight function, known as the PSF, decreases with distance to the scan point. The shape of the PSF mainly depends on the tip shape and tip-to-sample distance.

In order to simulate the surface potential measured by KPFM, the PSF is applied to the surface potential distribution centered at the tip coordinate for every tip position. As described in Ref. 21, the weight factors are given by the z-derivative of the tip/sample capacitances $C_{i,t}$, assuming that the sample surface consists of n small ideal conducting electrodes of potential ϕ_i. Hence, the link between the measured surface potential at the tip position, ϕ_t, and the surface potential at the i'th electrode is given by

$$\phi_t = \sum_{i=1}^{n}\left(\frac{dC_{i,t}}{dz}\phi_i\right) \Big/ \sum_{i=1}^{n}\frac{dC_{i,t}}{dz}. \quad (4)$$

The capacitance gradients are functions of the lateral distance r between the position of the tip and the *ith* electrode. These are obtained from COMSOL Multiphysics 4.3 using the tip geometry parameters listed in Table II.

IV. RESULTS AND DISCUSSION

A. AFM and KPFM measurements

The images of AFM and KPFM measurements on the test sample are shown in Figs. 3(a) and 3(b), respectively. From the AFM results, it is observed that there is a height difference of approximately 80–100 nm between areas with and without the metal stripes (top panel of Fig. 3(c)), confirming that the PMMA film follows the sample geometry shown in Fig. 2.

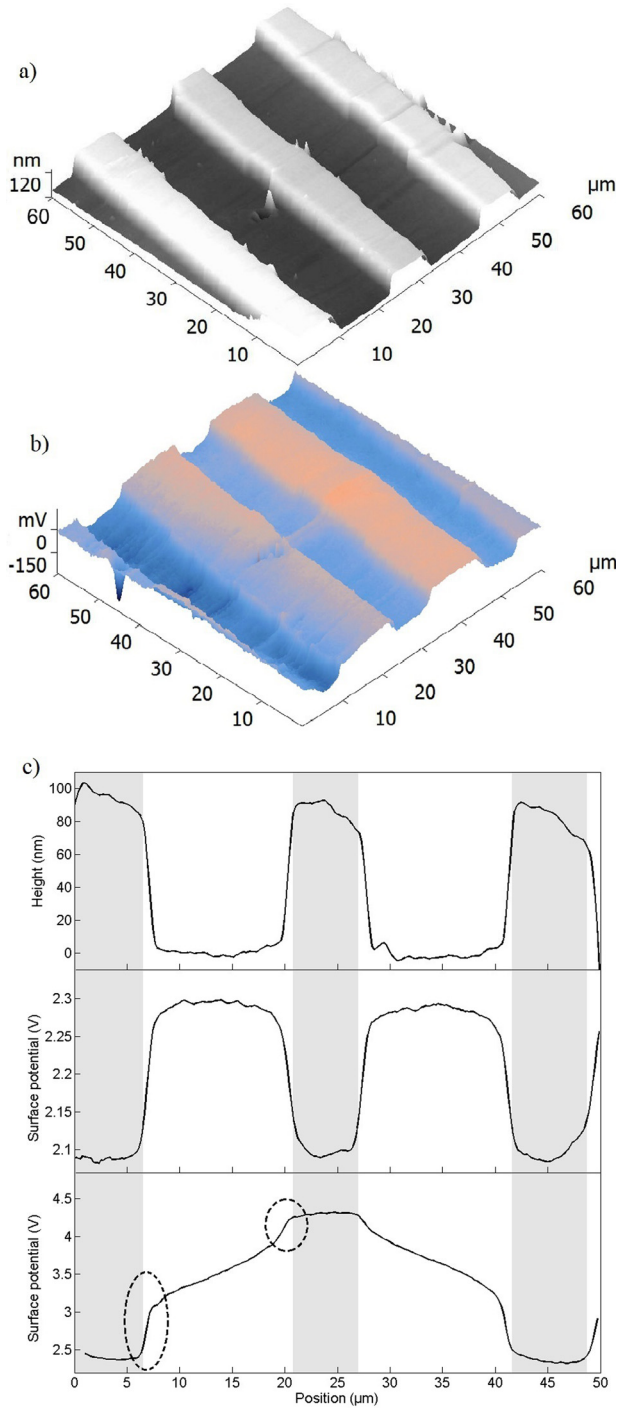

FIG. 3. (a) and (b) 3D images of the AFM and KPFM measurements, respectively. (c) Line profiles of the sample topography (top), measured surface potential with both grids grounded (middle), and measured surface potential with 3 V applied to one of the grids with the other one grounded (bottom). The gray areas represent the positions of the metal stripes and the two ellipses in the bottom panel highlight the potential evolution at the electrode edges.

The KPFM measurements on the test sample with both grids grounded show a periodic surface potential distribution (middle panel of Fig. 3(c)) corresponding to the sample geometry with lower surface potential on PMMA with underlying metal stripes. The difference in surface potential between the areas on the stripes and those on the glass is measured to be approximately 190 mV. During this measurement, the CPD between the tip and the aluminum grid was found to be 2.05 V. This could indicate surface oxidation of the aluminum stripes, because the CPD between PtIr and pure aluminum should be around −1.2 V. The CPD between PtIr and aluminum oxide, on the other hand, is about 1.7 V,[22,23] which is close to the measured value. Energy-dispersive x-ray spectroscopy measurements on a sample without PMMA confirm the suggestion about oxidation by showing a high concentration of oxygen on an aluminum stripe, which is most likely to be caused by the wire soldering process to make contacts to the grid.

For the case of 3 V applied to one of the grids with the other one grounded, the potential difference between the biased and grounded stripes is measured to be around 1.9 V (see bottom panel of Fig. 3(c)) instead of expected 3 V. It is also observed that the potential gradient, i.e., the steepness of the potential profile, is considerably larger at the grounded strip edges compared to those with 3 V applied. These areas are marked by ovals in the bottom panel of Fig. 3(c). Both effects are suggested to be caused by the tip-induced polarization of the dielectric. The induced polarization field counteracts the externally applied field thus reducing the measured potential difference. It is obvious that this effect will be greatest around the grounded stripes, where the polarization is the strongest, which is experimentally found as the highest gradient. It is worth noting that the higher gradient will always be at the grounded stripe edges also if the bias direction is switched.

B. Simulation results

1. Surface potential distribution

The individual surface potential distributions for the sample with 3 V applied to one of the grids with the other one grounded without and with the presence of the tip at different positions are shown in Fig. 4. It is observed that the presence of the tip locally changes the potential profile and this change is significantly localized around the tip position as can be seen comparing Figs. 4(a)–4(d). This is a clear indication how the induced polarization field affects the local surface potential. Summary of individual profiles is given in Fig. 4(e), and this type of profile is expected from KPFM measurement on the biased test sample. It can clearly be seen that the polarization caused by the tip leads to significant overall change of the potential profile. It should be noted that the point spread function has not yet been applied to the simulation results.

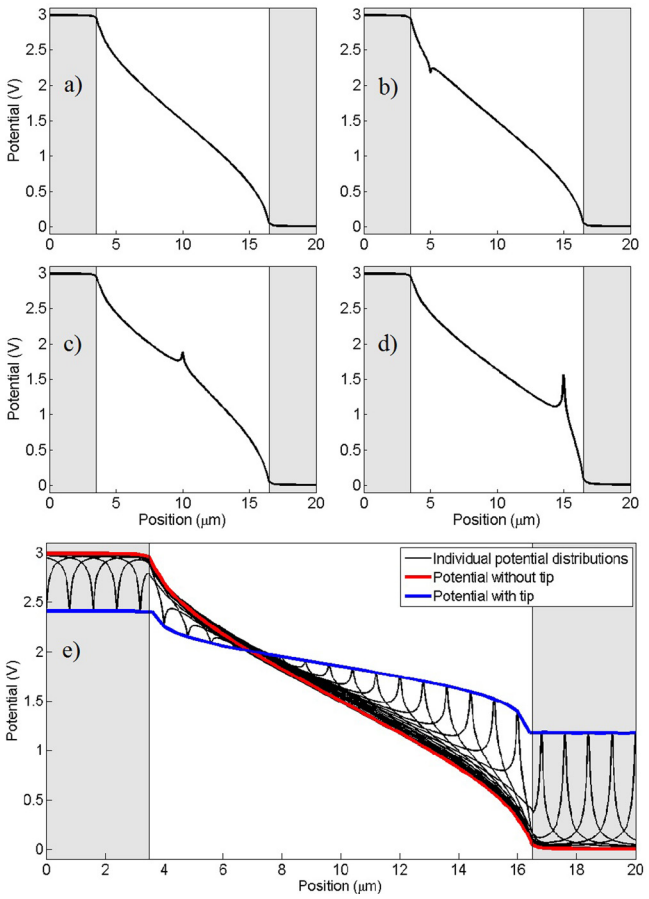

FIG. 4. Line profiles of the simulated potential distributions on the surface of the PMMA layer with 3 V applied to one of the grids with the other one grounded (a) without the cantilever tip, (b) with tip positioned at 5 μm, (c) with tip positioned at 10 μm, and (d) with tip positioned at 15 μm. (e) Profile of the surface potential for the case without tip and with the tip moving with intervals of 2 μm. Individual surface potential profiles for every tip position are shown as well.

2. Point spread function

The PSFs (capacitance gradients) for the tip at $z = 10$, 20, 30, and 50 nm were obtained from COMSOL and using Eq. (4). The data are fitted to the following equation:

$$PSF(r;z) = a(z)\frac{\tanh(b(z)\cdot r)}{b(z)\cdot r + c(z)\cdot r^3}, \tag{5}$$

where a is the normalization parameter, b and c are the shape parameters, and r is the lateral distance from the tip position to the calculated point in nanometres. It is fitted with $r^2 > 0.999$ to the generated PSF data as shown in Fig. 5. It fulfills the requirement that

$$\left.\frac{dPSF(r;z)}{dr}\right|_{r\to 0} = 0, \tag{6}$$

which ensures that there is no discontinuity at $r = 0$. It should be noted that Eq. (5) has no physical origin, but merely is an appropriate function for describing the PSFs for the cantilever tip obtained by simulations.

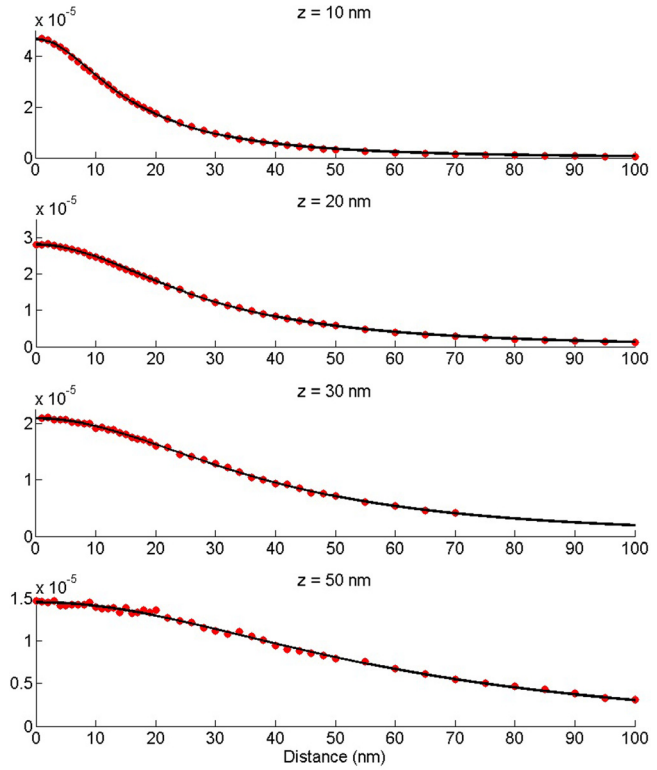

FIG. 5. PSF simulation data (•) and fit lines (-) as a function of the tip-to-sample distance. The simulations are carried out for 4 different vertical distances: 10, 20, 30, and 50 nm.

The shape parameters and full-with-half-maximum (FWHM) values of the PSFs at the different tip-to-sample distances are listed in Table III. The FWHMs of the PSFs generated in this work are comparable to those derived by Cohen *et al.*[24]

It should be stressed that the PSFs are generated for a conical tip with a hemispherical apex of $R = 35$, which is chosen due to manufacturer specifications and represents an ideal case. In used cantilevers, the tips are gradually worn that leads to increase of apex radius, which will cause a broader PSF as shown by Strassburg *et al.*[25] Also, different tip shapes and sizes would need to use different PSFs; however, this is not considered in this study.

C. Measurement and simulation comparison

The results of the surface potential simulation with both grids grounded and the KPFM measurements are compared in Fig. 6. At this point, the PSF has been applied in the

TABLE III. Shape parameters and FWHM of the PSFs for the different tip-to-sample distances.

z (nm)	b (10^{-3} nm^{-1})	c (10^{-6} nm^{-3})	*FWHM* (nm)
10	107.4	62.79	30.4
20	56.76	16.34	53.1
30	39.64	6.782	73.5
50	9.538	2.539	111.4

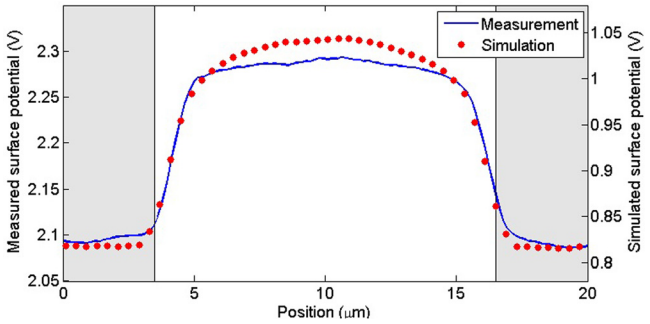

FIG. 6. Measured and simulated surface potential distributions for the sample with both grids grounded. The gray areas at left and right correspond to aluminum stripes.

simulations. It is observed that the measurement and simulation match fairly well.

The experimental and simulated results for the biased case are shown in Fig. 7. Again, it is seen that there is a good agreement between the model and the experiment, demonstrating that both correct surface potential values and profile of the potential can be accurately predicted. It is worth stressing that the tip induced polarization of the PMMA film is taken into account in the simulations.

In order to emphasize the difference between the actual (without tip, i.e., no tip-induced polarization) and the measured (with tip) surface potential distributions, a comparison is shown in Fig. 8, for the case of 3 V bias applied to one of the grids (left stripe in the figure). By comparing the profiles with and without the tip, it is clearly seen how the tip affects the measurement. It is observed that the presence of the tip causes larger gradients at the stripe edges compared to the case without the tip and leads to a decrease of the surface potential difference between two neighboring metal stripes from 3 V to 1.85 V. This value is in good agreement with the measured one (see bottom profile in Fig. 3(c)).

For comparison of our modelling with the method used in Ref. 17, which is briefly mentioned in the introduction, we simulated the case where the surface potential for grounded grids is subtracted from that of the biased one. It is the profile called "0 V subtracted" in Fig. 8, and it is significantly different from the profile without the tip (solid curve), which it was intended to reproduce. It is seen that the approach reduces the absolute value of the surface potential profile (short dash

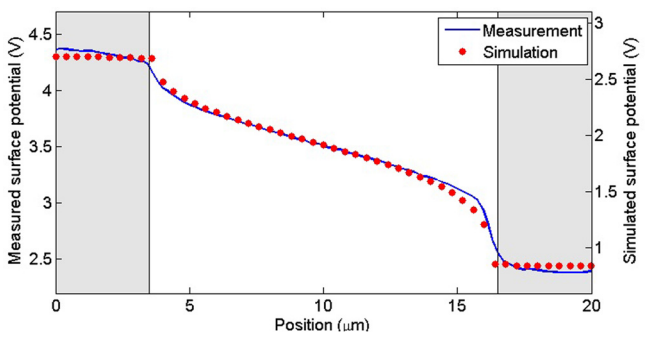

FIG. 7. Measured and simulated surface potential distributions for the sample with 3 V DC applied to the left stripe.

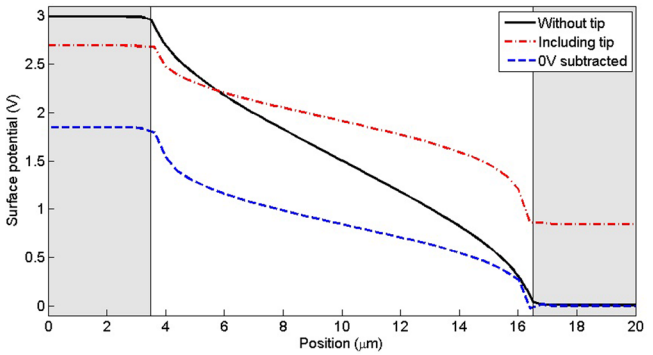

FIG. 8. Simulated surface potential distributions with 3 V applied without the tip, with the tip, and with the 0 V distribution subtracted (see details in the text about the subtraction procedure).

curve), but maintains the potential difference between the left and right stripes similar to that simulated with consideration of polarization (dash-dot line). Furthermore, it does not reproduce the potential gradients at the edge of the stripes correctly. Thus, this method can lead to misinterpretation of the obtained KPFM results, especially at the interfaces.

V. CONCLUSION

In this work, we have developed an approach to predict the surface potential distribution on metal/dielectric heterostructures measured by KPFM. The test samples have been designed to consist of two interleaving grids of aluminum stripes deposited on glass substrate and covered by a thin PMMA film. We have shown how the cantilever tip locally changes both the value of the electrostatic surface potential of a dielectric film and the gradient of the potential at interfaces. Good qualitative and quantitative agreement between experimental and simulation results is obtained on the test structures and corresponding model configurations. It has been concluded that the high potential gradients at the interfaces as well as the resulting map of the measured surface potential are highly affected by the additional polarization of the dielectric caused by the tip. This polarization field can be easily isolated in the modelling giving a possibility to quantify its contribution in the experiments. Thus, the approach introduces a physics-based explanation of the electric phenomena under the KPFM measurements on dielectrics and relates them to possible distortions in the recorded data. The model also allows to eliminate speculations in the interpretation of the results concerning effects caused by charges/currents, such as contact resistance or potential barriers.

As a final remark, it should be noted that the model constructed in this work is merely the first step toward a better understanding of the effect of tip-induced polarization that arises during KPFM on metal/dielectric heterostructures. It enables prediction of the measured surface potential distribution on certain structures as well as simulation of the potential that would exist without the tip-induced polarization. As the next step, we see the development of a dynamic model that deals with the force on the cantilever from the polarized dielectric, thus allowing the reconstruction of "true" surface potential from the measured one.

ACKNOWLEDGMENTS

This work is a part of the research activity within the Center of Reliable Power Electronics (CORPE) funded by the Innovation Fund Denmark.

[1]H.-J. Butt, B. Cappella, and M. Kappl, Surf. Sci. Rep. **59**, 1–152 (2005).
[2]Y. Gan, Surf. Sci. Rep. **64**, 99–121 (2009).
[3]S. V. Kalinin, R. Shao, and D. A. Bonnell, J. Am. Ceram. Soc. **88**, 1077–1098 (2005).
[4]R. A. Oliver, Rep. Prog. Phys. **71**, 076501 (2008).
[5]W. Melitz, J. Shen, A. C. Kummel, and S. Lee, Surf. Sci. Rep. **66**, 1–27 (2011).
[6]C. Barth, A. S. Foster, C. R. Henry, and A. L. Shluger, Adv. Mater. **23**, 477–501 (2011).
[7]T. Glatzel, M. Lux-Steiner, E. Strassburg, A. Boag, and Y. Rosenwaks, in *Scanning Probe Microscopy*, edited by S. Kalinin and A. Gruverman (Springer Verlag, Berlin, 2007), p. 113.
[8]Y. Rosenwaks, R. Shikler, T. Glatzel, and S. Sadewasser, Phys. Rev. B **70**, 085320 (2004).
[9]H. Huang, H. Wang, J. Zhang, and D. Yan, Appl. Phys. A **95**, 125–130 (2009).
[10]C. Baumgart, M. Helm, and H. Schmidt, Phys. Rev. B **80**, 085305 (2009).
[11]S. Magonov, J. Alexander, and S. Wu, in *Scanning Probe Microscopy of Functional Materials*, edited by S. Kalinin and A. Gruverman (Springer Verlag, Berlin, 2010), p. 223.
[12]C. Barth and C. R. Henry, Phys. Rev. Lett. **98**, 136804 (2007).
[13]T. Okamoto, S. Kitagawa, N. Inoue, and A. Ando, Appl. Phys. Lett. **98**, 072905 (2011).
[14]A. Kalabukhov, Y. A. Boikov, I. Serenkov, V. Sakharov, V. Popok, R. Gunnarsson, J. Börjesson, N. Ljustina, E. Olsson, D. Winkler, and T. Claeson, Phys. Rev. Lett. **103**, 146101 (2009).
[15]V. N. Popok, A. Kalabukhov, R. Gunnarsson, S. Lemeshko, T. Claeson, and D. Winkler, J. Adv. Microsc. Res. **5**, 26–30 (2010).
[16]C. Barth and C. R. Henry, J. Phys. Chem. C **113**, 247–253 (2009).
[17]L. Bürgi, H. Sirringhaus, and R. Friend, Appl. Phys. Lett. **80**, 2913–2915 (2002).
[18]C.-S. Jiang, H. Moutinho, D. Friedman, J. Geisz, and M. Al-Jassim, J. Appl. Phys. **93**, 10035–10040 (2003).
[19]C. Musumeci, A. Liscio, V. Palermo, and P. Samorì, Mater. Today **17**, 504–517 (2014).
[20]G. Elias, T. Glatzel, E. Meyer, and Y. Rosenwaks, Beilstein J. Nanotechnol. **2**, 252–260 (2011).
[21]V. Palermo, M. Palma, and P. Samorì, Adv. Mater. **18**, 145–164 (2006).
[22]D. E. Eastman, Phys. Rev. B **2**, 1 (1970).
[23]A. M. Goodman, J. Appl. Phys. **41**, 2176–2179 (1970).
[24]G. Cohen, E. Halpern, S. U. Nanayakkara, J. M. Luther, C. Held, R. Bennewitz, A. Boag, and Y. Rosenwaks, Nanotechnology **24**, 295702 (2013).
[25]E. Strassburg, A. Boag, and Y. Rosenwaks, Rev. Sci. Instrum. **76**, 083705 (2005).